ACS Sustainable Chemistry & Engineering

Research Article

Cite This: ACS Sustainable Chem. Eng. XXXX, XXX, XXX−XXX

pubs.acs.org/journal/ascecg

Synthesis of Biomass-Derived Nitrogen-Doped Porous Carbon Nanosheests for High-Performance Supercapacitors

Lu Guan, Lei Pan, Tingyue Peng, Cai Gao, Weinan Zhao, Zhongxue Yang, Han Hu,* and Mingbo Wu*

State Key Laboratory of Heavy Oil Processing, Institute of New Energy, College of Chemical Engineering, China University of Petroleum (East China), No. 66, West Changjiang Road, Huangdao District, Qingdao 266580, China

Supporting Information

ABSTRACT: Graphene-like two-dimensional carbon nanosheets with properly modulated compositions and porosity are of particular importance for robust capacitance harvesting. Nevertheless, the large-scale and cost-effective production of such nanostructures still remains a great challenge. Herein, we innovatively produce nitrogen-doped porous carbon nanosheets using pine nut shells, an abundant biomass waste, as the precursor, under the synergetic effect of KOH and melamine during the activation process. The sole activation of the precursors with KOH can produce only traditional activated carbon particles of several micrometers, while interestingly, the extra introduction of melamine results in nitrogen-doped porous carbon nanosheets possessing high tunability. By construction of a two-electrode configuration, the supercapacitors with optimal nanosheets as the electrode materials can deliver a superior specific capacitance of 324 F g^{-1} at 0.05 A g^{-1}, outstanding rate capability of 258 F g^{-1} at 20 A g^{-1}, and extraordinary cyclic stability of 94.6% after 10 000 cycles at 2 A g^{-1} in an aqueous electrolyte of 6 M KOH. Such a facile strategy proposed here may contribute to new possibilities of synthesizing graphene-like porous carbon nanosheets in a sustainable manner for energy-related applications.

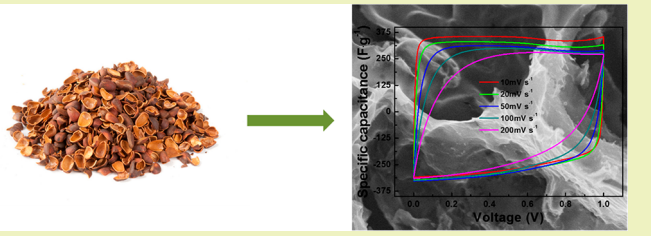

KEYWORDS: *Biomass, Nitrogen doping, Synergetic effect, Graphene-like porous carbon, Supercapacitor*

INTRODUCTION

The imminent shortage of fossil fuel and increasing concerns about environmental pollution call for innovation of energy storage devices to address these urgent issues. Supercapacitors are a promising type of energy storage devices because of their advantages, such as superior cycliability and extraordinary power density.[1,2] These merits make supercapacitors a potential candidate to partially or fully replace the dominating lithium ion batteries in many current and emerging applications.[3,4] Typically, porous carbon materials are the primary candidate of supercapacitive energy storage materials, where the large specific surface area, rich porosity, and outstanding conductivity could contribute to rapid adsorption/desorption of ions via an electrical double-layer mechanism.[5−7] Nevertheless, the practical performance of these porous carbon-based supercapacitors largely lags behind the continuously increasing demand of the current and emerging applications because of the deteriorated ion transport in tortuous pores at large current densities. As a result, one effective strategy in boosting the capacitive energy harvesting of carbon materials is to manipulate them into an atomic-thick structure with open porosity, for example, graphene.[8,9] Compared to the widely employed particulate-type carbon materials, graphene-based electrodes can secure fast and effective ion transport, thus contributing to outstanding energy storage performance.[10−13] In the past decade, graphene has been extensively investigated for this purpose with remarkable progress achieved. Meanwhile, the rising of graphene in this field has also promoted research interest and application of other two-dimensional carbon nanomaterials including carbon nanoplates[14,15] and carbon nanosheets.[16]

From a viewpoint of sustainability, the pursuit of renewable carbon source and exploration of facile yet economical synthesis process are of particular importance in bringing graphene and their carbon-based analogues into real energy storage application.[17] Nevertheless, even the most economical strategies developed so far for graphene and graphene-like materials synthesis still cannot rival the production of activated carbon.[18] Naturally abundant biomass mainly consists of three components, namely, cellulose, hemicelluloses, and lignin, which represent the most widely used precursor for activated carbon production in a sustainable manner. Through the activation effect of KOH at elevated temperature, the biomass is converted into carbon materials, which usually exist in a particulate form with high specific surface area and rich porosity.[19] A meaningful prospect for propelling the real use of graphene and graphene-like materials is to synthesize them

Received: January 3, 2019
Revised: March 18, 2019
Published: March 27, 2019

DOI: 10.1021/acssuschemeng.9b00050
ACS Sustainable Chem. Eng. XXXX, XXX, XXX−XXX

using biomass through a simple process, which would then be essentially cost-competitive.

Many kinds of biomass, such as ant powder,[20] chicken eggshell,[21] garlic skin,[22] soybeans,[23] human hair,[24] and prawn shells,[25] have been extensively investigated as precursors for carbon materials. As one of the most abundant products in the food industry, pine nuts are consumed in tens of thousands of tons every year. Accordingly, quite a large amount of pine nut shells are also produced, which mainly end in low-value application. This will cause a great waste of resources and increase the burden on our environment. Table S1 (Supporting Information) reveals that the pine nut shell contains a higher content of fixed carbon than many other kinds of biomass for activated carbon production. Thus, the pine nut shell may be a promising raw material with the characteristic of higher yield for preparing carbon materials. Besides, pine nut shells possess high oxygen content and a certain amount of nitrogen (Table S2). The carbonization of biomaterials may allow its own oxygen and nitrogen to be inherited by the final carbon product for enhanced electrochemical performance. Herein, we demonstrate the employment of a mildly modified KOH activation process to produce nitrogen-doped porous carbon nanosheets (PCNs) using pine nut shells as the raw materials. After a simple washing and precarbonization, the as-obtained materials are mixed with KOH as well as melamine for activation. Because of the structural and compositional merits, the nitrogen-doped porous carbon nanosheets afford outstanding performance for capacitance energy harvesting. The strategy suggested here may inspire new possibility of sustainably producing graphene and graphene-like materials for advanced energy storage.

EXPERIMENTAL SECTION

Materials. Pine nut shells were obtained from northeast China. KOH and melamine were bought from Sinopharm Ltd. and Aladdin Ltd., respectively. All of the chemicals employed in our research were directly used as received without further treatment.

Synthesis of PCNs from Pine Nut Shell. First, the pine nut shells were washed with distilled water and ethanol to remove the impurities before drying at 60 °C for 12 h. Then these shells were pulverized into powder with sizes of less than 0.125 mm. After that, these powders were annealed in an inert atmosphere at 600 °C for 1 h. After another pulverization process, these fine powders, KOH, and melamine were mixed at different mass ratios (1:3:0, 1:3:0.5, 1:3:1, and 1:3:2), which were activated at 800 °C for 2 h. The PCNs were harvested via repeated washing with deionized water and diluted HCl solution (10%) before drying at 60 °C for 12 h. The PCNs synthesized at different conditions are named as PCN_{X-Y-Z}, where X, Y, and Z are the mass ratios of precarbonized pine nut shells, KOH, and melamine, respectively.

Material Characterizations. The microstructures of the PCNs were examined with an X'Pert PRO MPD X-ray diffractometer. An Hitachi S-4800 scanning electron microscope (SEM) and JEM-2100UHR transmission electron microscope (TEM) were employed to investigate the microstructure and morphology of PCNs. An ASAP 2020 Micropore Analyzer was employed to analyze the specific surface area and porosity of the PCNs. On the basis of the isotherms, the Brunauer–Emmett–Teller (BET) method and density functional theory method were used to calculate the specific surface area (S_{BET}) and pore size distribution, respectively. Then the equation $D_{ap} = 4V_t/S_{BET}$ was used to determine the average pore diameter (D_{ap}). The doping state of the heteratoms in PCNs were investigated using a Thermo ESCALAB250 X-ray photoelectron spectroscope. The defects of the PCNs were examined using a Raman spectrometer (Renishaw RM2000).

Electrochemical Measurements. The slurry of the working electrode was made by mixing the PCNs and polymer binder, polytetrafluoroethylene (PTFE), with a mass ratio of 9:1 in an organic *N*-methyl-2-pyrrolidone solvent. The as-prepared slurry was then coated onto nickel foams followed by drying in a vacuum oven at 60 °C for 12 h. The supercapacitive performance of the electrode materials was first evaluated using a three-electrode configuration where the platinum foil serves as the counter electrode and Hg/HgO electrode is used as the reference electrode in an aqueous electrolyte of 6 M KOH. Then two carbon electrodes with equal mass were employed to construct a supercapacitor operated both in aqueous electrolytes of 6 M KOH and 1 M Na_2SO_4, separately. Cyclic voltammetry (CV) curves and galvanostatic charge–discharge (GCD) profiles were recorded with a CHI760E electrochemical workstation (Chenhua, Shanghai, China). Nyquist plots of both the electrode materials and the supercapacitors were obtained with an Ametek PARSTAT4000 electrochemistry workstation in a frequency span ranging from 100 kHz to 10 mHz with an alternating current voltage amplitude of 5 mV. The cycliability was evaluated using Arbin Instruments.

In the three-electrode configuration, the gravimetric capacitances were obtained from discharge portion of GCD curves based on the following equation:

$$C_s = \frac{I\Delta t}{m\Delta V} \tag{1}$$

In eq 1, C_s (F g^{-1}) represents the specific capacitance of the electrode materials, I (A) is the discharging current, Δt (s) describes the time for full discharge, m (g) is the loading amount of the active species, and ΔV (V) expresses the width of the potential window.

The gravimetric specific capacitance of the carbon electrode materials was also calculated from the two-electrode configuration and the equation used is described as follows:

$$C_s = \frac{4I\Delta t}{m\Delta V} \tag{2}$$

The difference in these two equations is that m (g) in eq 2 contains the mass of active species from both positive and negative electrodes in the two-electrode configuration. Then the energy density (E, W h kg^{-1}) and power capability (P, W kg^{-1}) of the as-prepared supercapacitors were obtained via the following equation:

$$E = \frac{1}{2 \times 4 \times 3.6} C_s V^2 \tag{3}$$

$$P = \frac{E}{\Delta t} \tag{4}$$

where C_s (F g^{-1}) means the specific capacitance of the supercapacitors, V (V) is the usable potential window (excluding IR drop), and t (h) describes the time for full discharge.

RESULTS AND DISCUSSION

The employment of melamine is of particular importance in producing the two-dimensional carbon nanosheets. Without melamine, the activation of the precarbonized pine nut shell (Figure S1a) using KOH can produce only carbon particulates of several micrometers (Figure S1b and Figure 1a), similar to typical activated carbon.[19] When melamine is incorporated during the activation process, significant morphology changes have been observed (Figure 1b–d). The bulk carbon particles are first converted into a highly porous carbon framework (Figure 1b), which further evolve into interconnected carbon nanosheets (Figure 1c) and then discrete carbon nanosheets (Figure 1d) while gradually increasing the amount of melamine. The possible reason may be ascribed to the different stability of cellulose, hemicellulose, and lignin, the main components of the pine nut shell, under the activation

DOI: 10.1021/acssuschemeng.9b00050
ACS Sustainable Chem. Eng. XXXX, XXX, XXX–XXX

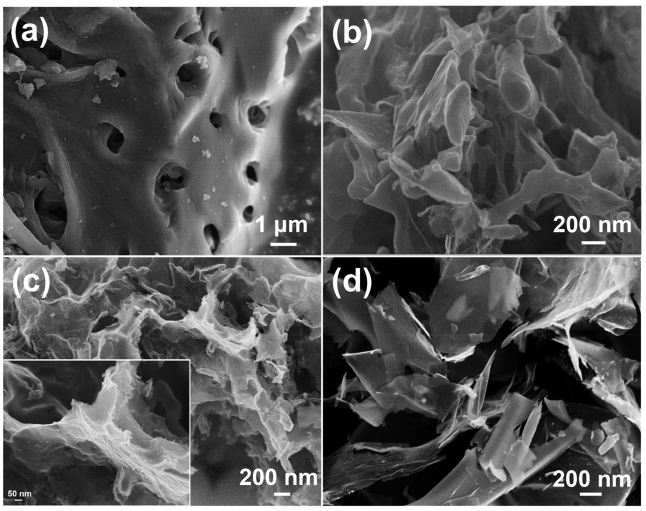

Figure 1. SEM images of (a) PCN_{1-3-0}, (b) $PCN_{1-3-0.5}$, (c) PCN_{1-3-1}, and (d) PCN_{1-3-2}. The inset in panel (c) is an SEM image of PCN_{1-3-1} at higher magnification.

process. The sole use of KOH may not be strong enough to etch the stable portion, resulting in bulk particles. The introduced melamine could condense into g-C_3N_4 (Figure S2), which would then be decomposed into many kinds of N-containing species, such as NH_3, $C_2N_2^+$, $C_3N_2^+$, and $C_3N_3^+$.[26] Probably, more carbon will be etched by these highly active species, leaving the most stable part behind in the form of two-dimensional carbon nanosheets.[27]

To obtain insightful understanding of the microstructure of the PCNs, XRD patterns and Raman profiles were recorded. The XRD patterns (Figure S3a) show diffraction peaks around 24° and 43°, which are due to the (002) and (101) planes, respectively. The very weak and broad peaks reveal that the as-prepared carbon materials are amorphous. These results coincide well with the Raman spectra where large I_D/I_G ratios are observed for all these samples (Figure S3b). Moreover, TEM observation was conducted to explore the structural and morphological details. As for the PCN_{1-3-1} exhibited in Figure 2a, the carbon nanosheets are almost transparent, indicative of the thin thickness. Such a structure can provide extremely small transport distance for ions. At higher magnification (Figure 2b), the nanosheet shows a micropore-dominated

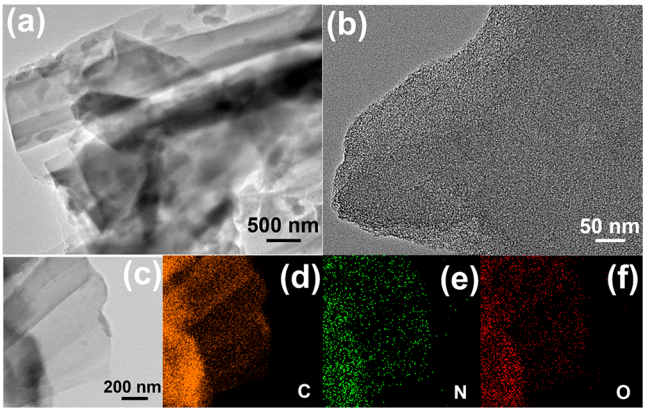

Figure 2. TEM images of PCN_{1-3-1} at low (a) and high resolution (b). Elemental mapping of an individual nanosheet (c) with uniformly distributed (d) C, (e) N, and (f) O.

surface, securing a large specific surface area and rich porosity, both of which are of particular importance for outstanding energy storage.[23] Then energy-dispersive X-ray (EDX) analysis (Figure 2c–f) was also performed, which revealed a uniform distribution of carbon, oxygen, and nitrogen.

The chemical state of these heteroatoms was further evaluated using X-ray photoelectron spectroscopy (XPS). As shown, all three typical samples, namely, $PCN_{1-3-0.5}$, PCN_{1-3-1}, and PCN_{1-3-2}, give three peaks which can be ascribed to carbon, nitrogen, and oxygen. These results coincide well with the EDX analysis. The high-resolution O 1s spectra could be divided into three peaks corresponding to carbon–oxygen double bond (531.9 ± 0.2 eV), chemisorbed oxygen (534.0 ± 0.2 eV), and carbon–oxygen single bond (533.4 ± 0.2 eV) (Figure S4).[28] The N 1s spectra were deconvoluted into four peaks, which are ascribed to pyridinic nitrogen (N-6, 398.2 ± 0.2 eV), pyrrolic nitrogen (N-5, 400.2 ± 0.2 eV), graphitic nitrogen (N-Q, 401.7 ± 0.2 eV), and pyridinic nitrogen oxide (N-X, 402.9 ± 0.2 eV) (Figure 3b and Figure S5).[20] Nitrogen and oxygen are supposed to improve the wettability of the carbon materials, which could boost the accessibility of the electrode surface for enhanced capacitive capability.[29−31] The detailed configuration of nitrogen is further illustrated in Table 1. Obviously, N-6 and N-5 represent the dominated species (about 70 at. %), which may come from melamine.[32] This may contribute to enhanced performance as the possibility of providing extra reversible faradic capacity in an alkaline aqueous solution by N-6 and N-5 species.[33] Besides, N-6 and N-Q combine two and three sp^2 carbon atoms, respectively, which contribute to a pair of electrons (Figure 3c). Such a structure can contribute to accelerated electron transfer and improved conductivity.[34] Because of the highest content of N-5, N-Q, and N-X in PCN_{1-3-1}, its electrochemical performance may be superior to that of other carbon materials. To explore the effect of doped nitrogen and oxygen on wettability, the contact angle measurement was implemented. The contact angle of PCN_{1-3-1}, as shown in Figure 3d, is 23.9°, indicating a hydrophilic feature, which can favor the full wetting of the active species.[35]

The specific surface area and pore size distribution of carbon materials, which are vital for electrochemical application, were deduced from the nitrogen sorption isotherms. In Figure 4a, all these sorption isotherms are a typical I shape. At the relative pressure lower than 0.01, the adsorbed volume of the three samples soar rapidly and are saturated soon, indicating abundant micropores existed. A small hysteresis loop in the medium pressure range is observed for all three carbons proves the existence a certain amount of mesopores.[36] The more detailed pore size distribution is illustrated in Figure 4b, which indicates that the pore size is mainly distributed between 0.5 and 1 nm, while a minor portion of pores shows diameter larger than 2 nm. Apparently, PCN_{1-3-1} is rich in this type of micropores. It has been demonstrated that the extremely small micropores, namely, less that 1 nm, can contribute to anomalous increase in capacitance because of desolvation.[37,38] On the basis of the detailed specific surface area and pore size informaion listed in Table 2, PCN_{1-3-1} may deliver the highest electrochemical performance.

To explore the capacitive capability of PCNs, the electrochemical measurements were performed in an aqueous electrolyte of 6 M KOH using three-electrode configuration. As shown in Figure 5a, all the PCNs show a rectangular CV

DOI: 10.1021/acssuschemeng.9b00050
ACS Sustainable Chem. Eng. XXXX, XXX, XXX−XXX

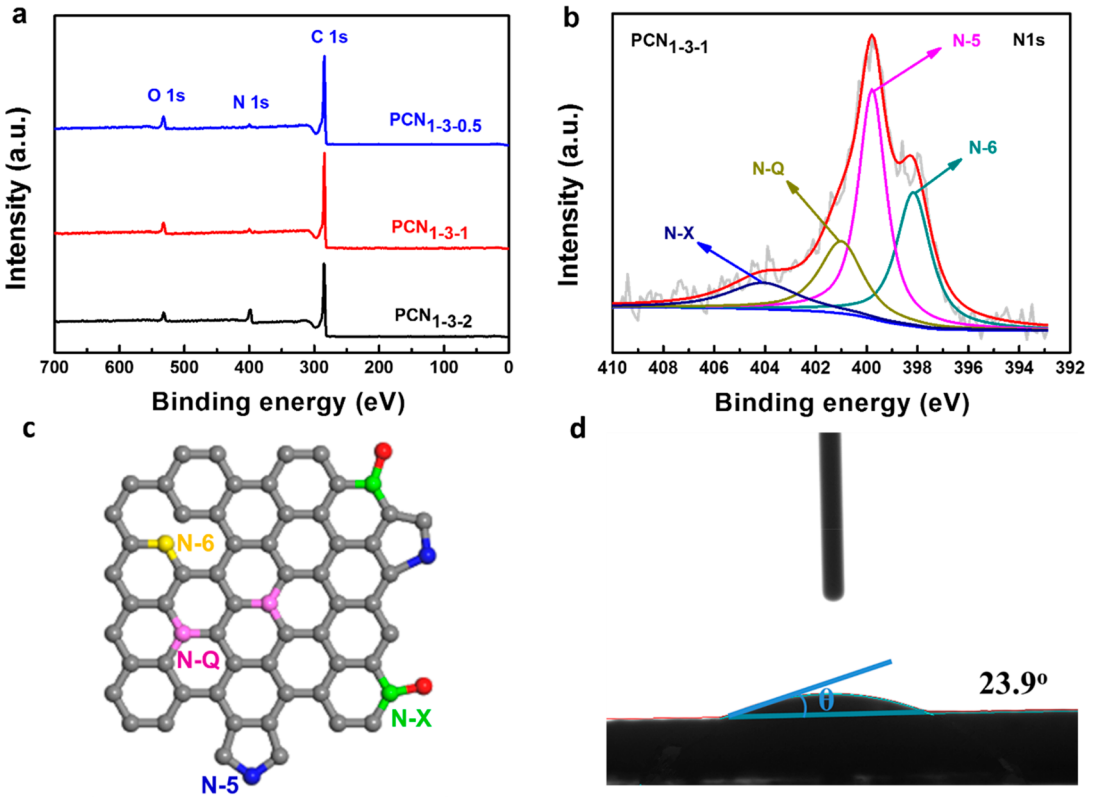

Figure 3. (a) Full range XPS spectra of $PCN_{1-3-0.5}$, PCN_{1-3-1}, and PCN_{1-3-2}. (b) N 1s spectrum of PCN_{1-3-1}. (c) Illustration of the possible locations of N in the carbon network. (d) Water contact angle measurement for the PCN_{1-3-1}.

Table 1. Nitrogen Configuration in PCNs

	% of total N 1s			
samples	N-6	N-5	N-Q	N-X
$PCN_{1-3-0.5}$	30.34	39.98	19.19	10.49
PCN_{1-3-1}	28.92	40.00	19.69	11.39
PCN_{1-3-2}	41.89	30.29	18.35	9.47

curve at a scan rate of 100 mV s^{-1} between −1 and 0 V (vs Hg/HgO), revealing a dominated electrical double-layer capacitance behavior. Minor peaks around −0.4 V (vs Hg/HgO) are observed which may be derived from the reversible redox reaction of heteroatoms. Obviously, the area of the PCN_{1-3-1} is larger than that of others, indicating that PCN_{1-3-1} delivers the highest specific capacitance. Then the CV curves of PCN_{1-3-1} at different scan rates ranging from 2 to 200 mV s^{-1} are compared in Figure 5b. Even at a scan rate up to 200 mV s^{-1}, rectanglar shape of the CV curves can be well-maintained which demonstrates excellent rate capability. Consistent with the CV results, all GCD curves (Figure 5c) are highly symmetric. Clearly, the specific capacitance of the PCN_{1-3-1} rivals that of other samples. The GCD curves of PCN_{1-3-1} were then further evaluated at different current densities to evaluate its rate performance. The excellent symmetry of the curves, as revealed in Figure 5d, can be delivered in a wide range from 0.5 to 20 A g^{-1}, demonstrating its excellent reversibility. Because of this, the excellent rate capability is secured as the capacitance retention can be as high as 74% (Figure S6a). Moreover, the almost absent voltage drop in the initial stage of discharge indicates the low internal

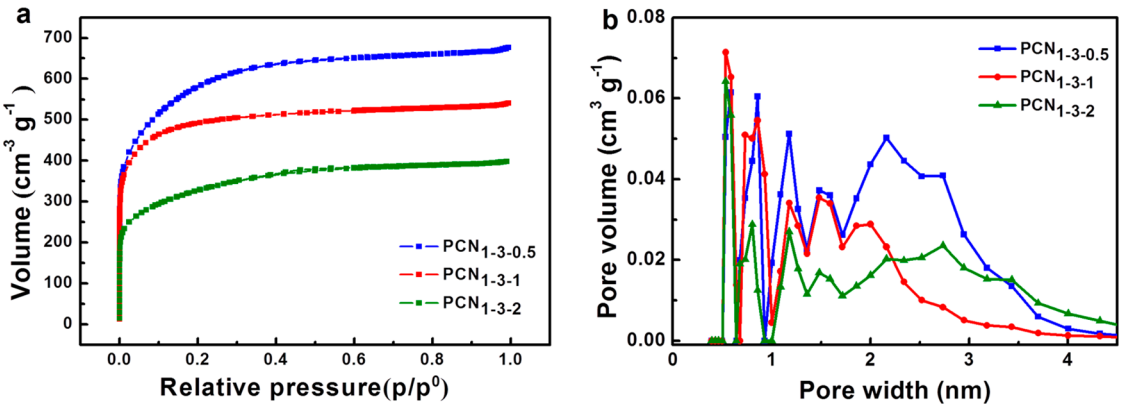

Figure 4. (a) N_2 sorption isotherms of PCNs and (b) their pore size distributions curves.

DOI: 10.1021/acssuschemeng.9b00050
ACS Sustainable Chem. Eng. XXXX, XXX, XXX−XXX

Table 2. Pore Structure Parameters of PCNs

sample	D_{ap} [nm]	S_{BET} [m^2 g^{-1}]	S_{mic} [m^2 g^{-1}]	V_t [cm^3 g^{-1}]	V_{mic} [cm^3 g^{-1}]	V_{mic}/V_t [%]
$PCN_{1-3-0.5}$	2.01	2093	2036	1.05	0.97	92.38
PCN_{1-3-1}	1.82	1847	1806	0.84	0.78	92.86
PCN_{1-3-2}	2.12	1167	1126	0.62	0.56	90.32

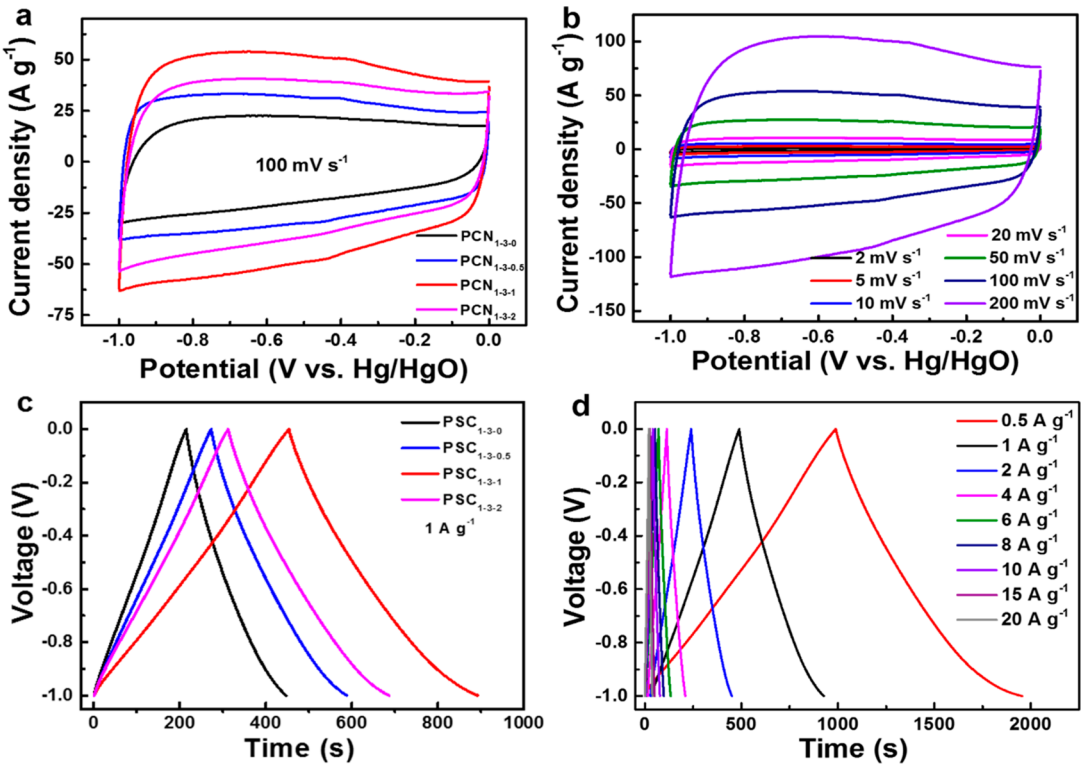

Figure 5. Electrochemical performance of PCNs evaluated in a three-electrode configuration. (a) CV curves of the PCNs recorded at a high scan rate of 100 mV s^{-1}. (b) CV profiles of PCN_{1-3-1} at scan rates ranging from 2 to 200 mV s^{-1}. (c) GCD curves of the PCNs obtained at a current density of 1 A g^{-1}. (d) GCD curves of PCN_{1-3-1} at current density ranging from 0.5 to 20 A g^{-1}.

resistance. This feature was further demonstrated through the electrochemical impedance measurements in Figure S6b. In the high-frequency region, the intercept is very small, demonstrating significant facilitated ion diffusion within the electrode. Moreover, the vertical nature of the curves at low frequency reveals an excellent capacitive feature. Obviously, PCN_{1-3-1} outperformances other PCNs through the comparison of their curves.

The PCNs-based supercapacitors were evaluated in a two-electrode system with an aqueous electrolyte of 6 M KOH. Figure 6a shows the CV curves of PCNs-based supercapacitors at a scan rate of 10 mV s^{-1}. Clearly, all of these CV curves exhibit a nearly rectangular shape, indicative of the dominated electrical double-layer capacitance (EDLC) behavior.[39] Obviously, the CV loop area of PCN_{1-3-1} is much larger than that of the other three samples, revealing its highest capacitance. To explore the rate capability of PCN_{1-3-1}, the CV evaluations were further measured at different scan rates ranging from 10 to 200 mV s^{-1}. The CV curve retains perfectly rectangular shape, even at a scan rate up to 200 mV s^{-1} (Figure 6b), indicating that the porous carbon nanosheets are suitable for rapid ion transfer. Then the GCD profiles of PCNs at a current density of 0.1 A g^{-1} were recorded. As shown in Figure 6c, all curves exhibit a typical triangle shape, suggesting desirable capacitive properties and electrochemical reversibility, which is in good agreement with the CV tests.[40] The rate performances of PCNs are compared in Figure 6d. Obviously, the PCN_{1-3-1} gives the highest specific capacitance of 324 F g^{-1}, while the value of PCN_{1-3-0}, $PCN_{1-3-0.5}$, and PCN_{1-3-2} is only 169, 207, and 264 F g^{-1}, respectively, at the current density of 0.05 A g^{-1}. The superior performance of PCN_{1-3-1} may be due to the ultrathin thickness, optimal pore structure, and high content of active nitrogen species. Figure 6e exhibits the Nyquist plots for PCNs in the frequency span of 0.01−100 kHz. Among all, PCN_{1-3-1} possesses the smallest semicircle in a high-frequency region. The equivalent circuit model was constructed to produce the calculated Nyquist plot (Cal) of PCN_{1-3-1}, which is compared favorably with the measured one (Msd). As shown in Figure 6f, the Msd and Cal plots almost overlapped each other, revealing the well-established equivalent circuit model for describing the whole supercapacitor circuit. Table S3 lists the detailed value of each circuit component, where R_s represents the equivalent series resistance, while R_{ct} and CPE describe the resistance of ion adsorption/desorption and the constant phase element, respectively. Notably, the value of R_s for PCN_{1-3-1} is only 0.64 ohm, referring to a low internal resistance and prominent conductivity. Furthermore, this sample displays an angle of 85.8° which is quite close to the ideal supercapacitors (90°) in Figure S7a. Additionally, 94.6% capacitance was retained after repeatedly charging and discharging at a current density of 2 A

DOI: 10.1021/acssuschemeng.9b00050
ACS Sustainable Chem. Eng. XXXX, XXX, XXX−XXX

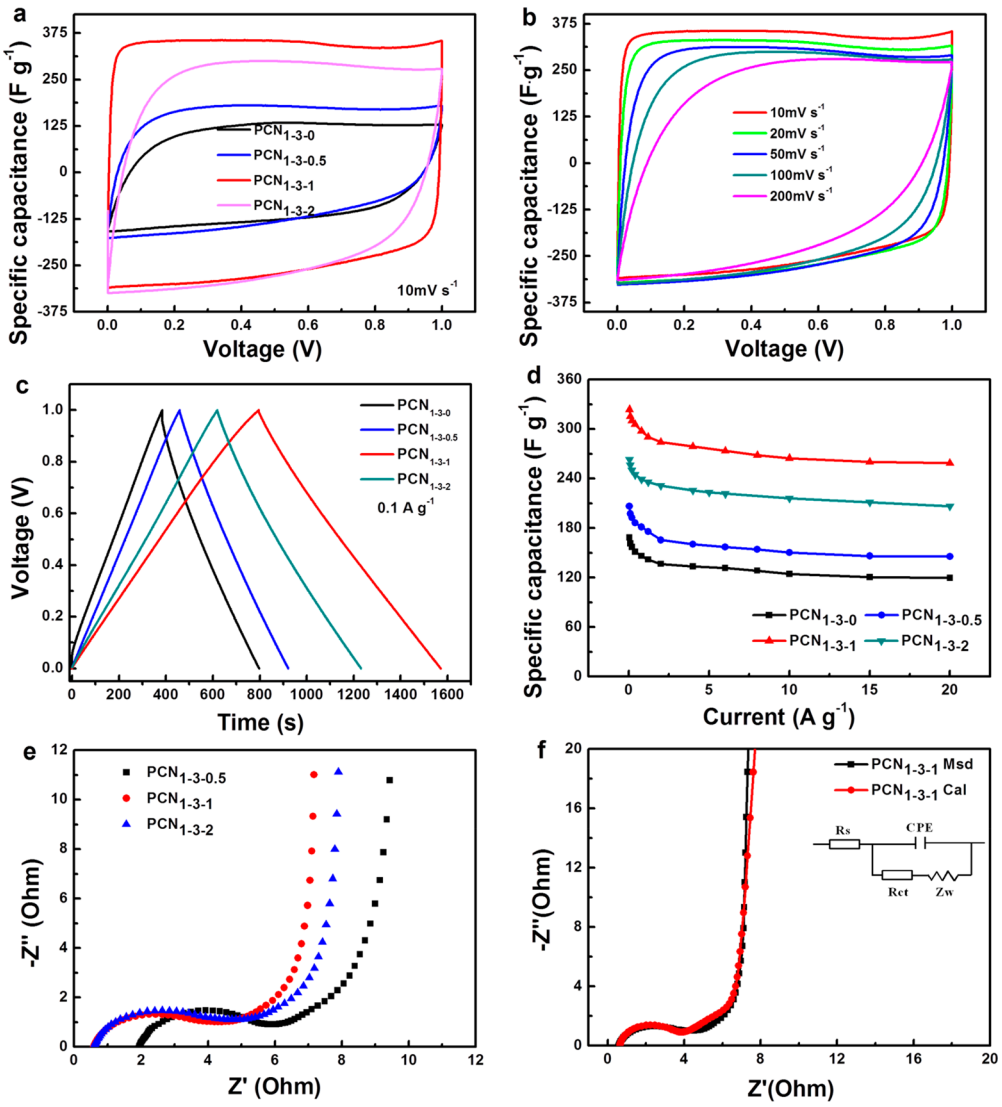

Figure 6. (a) CV curves of the PCNs at a scan rate of 10 mV s^{-1}. (b) CV curves of PCN_{1-3-1} at different scan rates (10, 20, 50, 100, and 200 mV s^{-1}). (c) GCD curves of the PCNs at a current density of 0.1 A g^{-1}. (d) Specific capacitance of PCNs at different current densities. (e) Nyquist plots of PCNs and (f) comparison of the measured Nyquist plot of PCN_{1-3-1} with the calculated one (insert is the equivalent circuit model).

g^{-1} for 10 000 cycles (Figure S7b), indicating the excellent calendar life of the PCNs-based supercapacitors.

The supercapacitors based on PCN_{1-3-1} were further evaluated in an aqueous electrolyte of 1 M Na_2SO_4. Because of the possibility of depressing oxygen evolution reaction and hydrogen evolution at cathode and anode, respectively, in neutral electrolytes, the employment of Na_2SO_4 electrolyte can essentially extend the working voltage window.[41] As revealed from CV curves in Figure 7a, the voltage window of such a supercapacitor can be as large as 1.8 V. Then the rate capability of the supercapacitors in a 1.8 V voltage window was measured. All GCD curves in Figure 7b show perfect symmetry, indicating good reversibility. The specific capacitance of PCN_{1-3-1} at a wide range of current densities is exhibited in Figure 7c. Specifically, a large specific capacitance of 110 F g^{-1} is delivered at a current density of 1 A g^{-1} while 56% of capacitance can be maintained with a 20-fold increase of current density. In the low-frequency region, the Nyquist plot (Figure S8) of a supercapacitor with PCN_{1-3-1} electrodes is nearly parallel to the imaginary axis ($-Z$) and the value of R_s, R_{ct}, and R_w is quite small, indicating high electrode conductivity and good electron-transfer rates. The Ragone plot reveals the energy density and power capability of the supercapacitors. As shown in Figure 7d, a very decent energy density of 11.9 W h kg^{-1} is achieved at a power density of 463.6 W kg^{-1}.

CONCLUSIONS

In summary, an efficient yet cost-effective strategy has been proposed to produce nitrogen-doped porous carbon nanosheets using pine nut shell, an earth-abundant biomass as the precursor, through the combined activation with KOH and melamine. Because of the low cost of precursor and facile process, such a strategy possesses great promise for being put into practice. Moreover, the structural merits of the as-prepared materials, such as appropriate pore size distribution and suitable heteroatom doping, are extremely needed for robust capacitive energy harvesting. Thus, the supercapacitor based on optimal carbon nanosheets delivers an attractive specific capacitance of 324 F g^{-1} at 0.05 A g^{-1}, and excellent rate capability, and long calendar life. This efficient yet facile route developed here may offer great benefits for mass

DOI: 10.1021/acssuschemeng.9b00050
ACS Sustainable Chem. Eng. XXXX, XXX, XXX−XXX

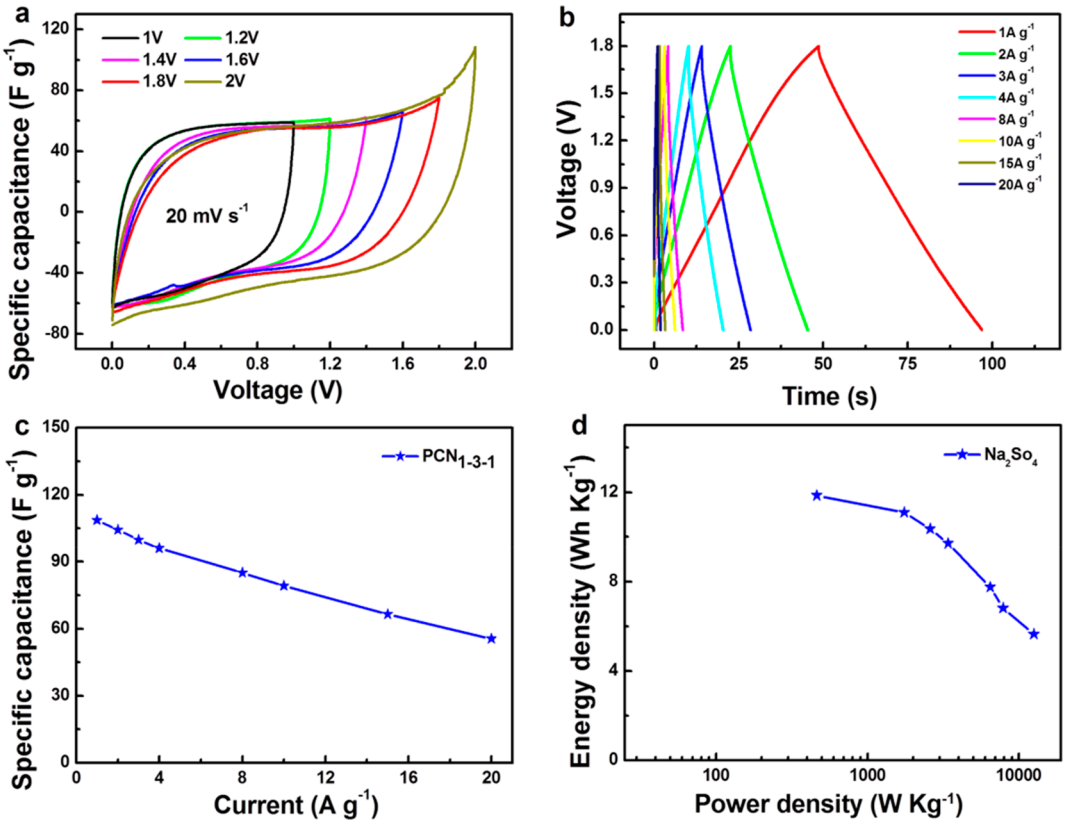

Figure 7. (a) CV curves of PCNs at a scan rate of 20 mV s^{-1} within different potential windows in an aqueous electrolyte of 1 M Na_2SO_4. (b) GCD curves and (c) the specific capacitance of PCNs-based supercapacitors at different current densities. (d) Ragone plot of the supercapacitor with PCN_{1-3-1} electrodes in a 1 M aqueous Na_2SO_4 electrolyte.

production of biomass-derived carbon nanomaterials for advanced energy storage.

■ ASSOCIATED CONTENT

Supporting Information

The Supporting Information is available free of charge on the ACS Publications website at DOI: 10.1021/acssuschemeng.9b00050.

Industry analysis, chemical composition, and element analysis of pine nut shell; FTIR, TG, and SEM; XRD and XPS; Bode plots, cycle stability, and EIS (PDF)

■ AUTHOR INFORMATION

Corresponding Authors

*E-mail: wumb@upc.edu.cn.
*E-mail: hhu@upc.edu.cn.

ORCID

Han Hu: 0000-0002-3755-7342
Mingbo Wu: 0000-0003-0048-778X

Notes

The authors declare no competing financial interest.

■ ACKNOWLEDGMENTS

The authors are grateful for the financial support from the National Natural Science Foundation of China (Nos. 51572296, U1662113), the Fundamental Research Funds for the Central Universities (15CX08005A), the Financial Support from Taishan Scholar Project (No. ts201712020), Technological Leading Scholar of 10000 Talent Project (No. W03020508), and Shandong Provincial Natural Science Foundation (ZR2018ZC1458), China.

■ REFERENCES

(1) Fan, Z.; Yan, J.; Zhi, L.; Zhang, Q.; Wei, T.; Feng, J.; Zhang, M.; Qian, W.; Wei, F. A three-dimensional carbon nanotube/graphene sandwich and its application as electrode in supercapacitors. *Adv. Mater.* **2010**, *22*, 3723−8.

(2) Hao, L.; Li, X.; Zhi, L. Carbonaceous electrode materials for supercapacitors. *Adv. Mater.* **2013**, *25*, 3899−904.

(3) Hall, P. J.; Mirzaeian, M.; Fletcher, S. I.; Sillars, F. B.; Rennie, A. J. R.; Shitta-Bey, G. O.; Wilson, G.; Cruden, A.; Carter, R. Energy storage in electrochemical capacitors: designing functional materials to improve performance. *Energy Environ. Sci.* **2010**, *3*, 1238.

(4) Wang, G.; Zhang, L.; Zhang, J. A review of electrode materials for electrochemical supercapacitors. *Chem. Soc. Rev.* **2012**, *41*, 797−828.

(5) Li, Q.; Hu, M.; Wang, K.; Wang, X. One-step approach for fabrication of 3D porous carbon/graphene composites as supercapacitor electrode materials. *Catal. Today* **2018**.

(6) Zhang, S.; Tian, K.; Cheng, B.-H.; Jiang, H. Preparation of N-Doped Supercapacitor Materials by Integrated Salt Templating and Silicon Hard Templating by Pyrolysis of Biomass Wastes. *ACS Sustainable Chem. Eng.* **2017**, *5*, 6682−6691.

(7) Ren, G.; Li, Y.; Chen, Q.; Qian, Y.; Zheng, J.; Zhu, Y.; Teng, C. Sepia-Derived N, P Co-doped Porous Carbon Spheres as Oxygen Reduction Reaction Electrocatalyst and Supercapacitor. *ACS Sustainable Chem. Eng.* **2018**, *6*, 16032−16038.

(8) Lim, L.; Liu, Y.; Liu, W.; Tjandra, R.; Rasenthiram, L.; Chen, Z.; Yu, A. All-in-One Graphene Based Composite Fiber: Toward Wearable Supercapacitor. *ACS Appl. Mater. Interfaces* **2017**, *9*, 39576−39583.

DOI: 10.1021/acssuschemeng.9b00050
ACS Sustainable Chem. Eng. XXXX, XXX, XXX−XXX

(9) Zhao, Y.; Liu, J.; Zheng, D.; Wang, B.; Hu, M.; Sha, J.; Li, Y. Achieving High Capacitance of Paper-Like Graphene Films by Adsorbing Molecules from Hydrolyzed Polyimide. *Small* **2018**, *14*, 1702809.
(10) Manjakkal, L.; Núñez, C. G.; Dang, W.; Dahiya, R. Flexible self-charging supercapacitor based on graphene-Ag-3D graphene foam electrodes. *Nano Energy* **2018**, *51*, 604−612.
(11) Bora, A.; Mohan, K.; Doley, S.; Dolui, S. K. Flexible Asymmetric Supercapacitor Based on Functionalized Reduced Graphene Oxide Aerogels with Wide Working Potential Window. *ACS Appl. Mater. Interfaces* **2018**, *10*, 7996−8009.
(12) El-Kady, M. F.; Strong, V.; Dubin, S.; Kaner, R. B. Laser scribing of high-performance and flexible graphene-based electrochemical capacitors. *Science* **2012**, *335*, 1326−30.
(13) Chen, W.; Yan, L. In situ self-assembly of mild chemical reduction graphene for three-dimensional architectures. *Nanoscale* **2011**, *3*, 3132−7.
(14) Golikand, A. N.; Bagherzadeh, M.; Shirazi, Z. Evaluation of the Polyaniline Based Nanocomposite Modified with Graphene Nanosheet, Carbon Nanotube, and Pt Nanoparticle as a Material for Supercapacitor. *Electrochim. Acta* **2017**, *247*, 116−124.
(15) Chao, Y.; Chen, S.; Chen, H.; Hu, X.; Ma, Y.; Gao, W.; Bai, Y. Densely packed porous graphene film for high volumetric performance supercapacitor. *Electrochim. Acta* **2018**, *276*, 118−124.
(16) Ding, B.; Guo, D.; Wang, Y.; Wu, X.; Fan, Z. Functionalized graphene nanosheets decorated on carbon nanotubes networks for high performance supercapacitors. *J. Power Sources* **2018**, *398*, 113−119.
(17) Ling, Z.; Wang, Z.; Zhang, M.; Yu, C.; Wang, G.; Dong, Y.; Liu, S.; Wang, Y.; Qiu, J. Sustainable Synthesis and Assembly of Biomass-Derived B/N Co-Doped Carbon Nanosheets with Ultrahigh Aspect Ratio for High-Performance Supercapacitors. *Adv. Funct. Mater.* **2016**, *26*, 111−119.
(18) Wang, K.; Pang, J.; Li, L.; Zhou, S.; Li, Y.; Zhang, T. Synthesis of hydrophobic carbon nanotubes/reduced graphene oxide composite films by flash light irradiation. *Front. Chem. Sci. Eng.* **2018**, *12*, 376−382.
(19) Gao, Z.; Zhang, Y.; Song, N.; Li, X. Biomass-derived renewable carbon materials for electrochemical energy storage. *Mater. Res. Lett.* **2017**, *5*, 69−88.
(20) Zhao, G.; Chen, C.; Yu, D.; Sun, L.; Yang, C.; Zhang, H.; Sun, Y.; Besenbacher, F.; Yu, M. One-step production of O-N-S co-doped three-dimensional hierarchical porous carbons for high-performance supercapacitors. *Nano Energy* **2018**, *47*, 547−555.
(21) Gao, F.; Qu, J.; Zhao, Z.; Wang, Z.; Qiu, J. Nitrogen-doped activated carbon derived from prawn shells for high-performance supercapacitors. *Electrochim. Acta* **2016**, *190*, 1134−1141.
(22) Zhang, Q.; Han, K.; Li, S.; Li, M.; Li, J.; Ren, K. Synthesis of garlic skin-derived 3D hierarchical porous carbon for high-performance supercapacitors. *Nanoscale* **2018**, *10*, 2427−2437.
(23) Long, C.; Jiang, L.; Wu, X.; Jiang, Y.; Yang, D.; Wang, C.; Wei, T.; Fan, Z. Facile synthesis of functionalized porous carbon with three-dimensional interconnected pore structure for high volumetric performance supercapacitors. *Carbon* **2015**, *93*, 412−420.
(24) Si, W.; Zhou, J.; Zhang, S.; Li, S.; Xing, W.; Zhuo, S. Tunable N-doped or dual N, S-doped activated hydrothermal carbons derived from human hair and glucose for supercapacitor applications. *Electrochim. Acta* **2013**, *107*, 397−405.
(25) Li, Z.; Zhang, L.; Amirkhiz, B. S.; Tan, X.; Xu, Z.; Wang, H.; Olsen, B. C.; Holt, C. M. B.; Mitlin, D. Carbonized Chicken Eggshell Membranes with 3D Architectures as High-Performance Electrode Materials for Supercapacitors. *Adv. Energy Mate.* **2012**, *2*, 431−437.
(26) Liu, Q.; Duan, Y.; Zhao, Q.; Pan, F.; Zhang, B.; Zhang, J. Direct synthesis of nitrogen-doped carbon nanosheets with high surface area and excellent oxygen reduction performance. *Langmuir* **2014**, *30*, 8238−45.
(27) Wang, H. L.; Xu, Z. W.; Kohandehghan, A.; Li, Z.; Cui, K.; Tan, X. H.; Stephenson, T. J.; King'ondu, C. K.; Holt, C. M. B.; Olsen, B. C.; et al. Interconnected Carbon Nanosheets Derived from Hemp for Ultrafast Supercapacitors with High Energy. *ACS Nano* **2013**, *7* (6), 5131−5141.
(28) Pan, L.; Wang, Y.; Hu, H.; Li, X.; Liu, J.; Guan, L.; Tian, W.; Wang, X.; Li, Y.; Wu, M. 3D self-assembly synthesis of hierarchical porous carbon from petroleum asphalt for supercapacitors. *Carbon* **2018**, *134*, 345−353.
(29) Li, Y.; Dong, J.; Zhang, J.; Zhao, X.; Yu, P.; Jin, L.; Zhang, Q. Nitrogen-Doped Carbon Membrane Derived from Polyimide as Free-Standing Electrodes for Flexible Supercapacitors. *Small* **2015**, *11*, 3476−84.
(30) Guo, C.; Li, N.; Ji, L.; Li, Y.; Yang, X.; Lu, Y.; Tu, Y. N- and O-doped carbonaceous nanotubes from polypyrrole for potential application in high-performance capacitance. *J. Power Sources* **2014**, *247*, 660−666.
(31) Hulicova-Jurcakova, D.; Kodama, M.; Shiraishi, S.; Hatori, H.; Zhu, Z. H.; Lu, G. Q. Nitrogen-Enriched Nonporous Carbon Electrodes with Extraordinary Supercapacitance. *Adv. Funct. Mater.* **2009**, *19*, 1800−1809.
(32) Wan, L.; Wang, J.; Xie, L.; Sun, Y.; Li, K. Nitrogen-enriched hierarchically porous carbons prepared from polybenzoxazine for high-performance supercapacitors. *ACS Appl. Mater. Interfaces* **2014**, *6*, 15583−96.
(33) Wei, X.; Li, Y.; Gao, S. Biomass-derived interconnected carbon nanoring electrochemical capacitors with high performance in both strongly acidic and alkaline electrolytes. *J. Mater. Chem. A* **2017**, *5*, 181−188.
(34) Wu, J.; Zhang, D.; Wang, Y.; Hou, B. Electrocatalytic activity of nitrogen-doped graphene synthesized via a one-pot hydrothermal process towards oxygen reduction reaction. *J. Power Sources* **2013**, *227*, 185−190.
(35) Zhao, J.; Lai, H.; Lyu, Z.; Jiang, Y.; Xie, K.; Wang, X.; Wu, Q.; Yang, L.; Jin, Z.; Ma, Y.; Liu, J.; Hu, Z. Hydrophilic Hierarchical Nitrogen-Doped Carbon Nanocages for Ultrahigh Supercapacitive Performance. *Adv. Mater.* **2015**, *27*, 3541−5.
(36) Xie, X.; He, X.; Shao, X.; Dong, S.; Xiao, N.; Qiu, J. Synthesis of layered microporous carbons from coal tar by directing, space-confinement and self-sacrificed template strategy for supercapacitors. *Electrochim. Acta* **2017**, *246*, 634−642.
(37) Chmiola, J.; Yushin, G.; Gogotsi, Y.; Portet, C.; Simon, P.; Taberna, P. L. Anomalous increase in carbon capacitance at pore sizes less than 1 nm. *Science* **2006**, *313* (5794), 1760−1763.
(38) Lin, R.; Taberna, P. L.; Chmiola, J.; Guay, D.; Gogotsi, Y.; Simon, P. Microelectrode Study of Pore Size, Ion Size, and Solvent Effects on the Charge/Discharge Behavior of Microporous Carbons for Electrical Double-Layer Capacitors. *J. Electrochem. Soc.* **2009**, *156*, A7.
(39) Choudhary, N.; Li, C.; Moore, J.; Nagaiah, N.; Zhai, L.; Jung, Y.; Thomas, J. Asymmetric Supercapacitor Electrodes and Devices. *Adv. Mater.* **2017**, *29*, 1605336.
(40) Gong, C.; Wang, X.; Ma, D.; Chen, H.; Zhang, S.; Liao, Z. Microporous carbon from a biological waste-stiff silkworm for capacitive energy storage. *Electrochim. Acta* **2016**, *220*, 331−339.
(41) Mondal, A. K.; Kretschmer, K.; Zhao, Y.; Liu, H.; Fan, H.; Wang, G. Naturally nitrogen doped porous carbon derived from waste shrimp shells for high-performance lithium ion batteries and supercapacitors. *Microporous Mesoporous Mater.* **2017**, *246*, 72.

DOI: 10.1021/acssuschemeng.9b00050
ACS Sustainable Chem. Eng. XXXX, XXX, XXX−XXX